

# ***In Vivo* Parametric T1 Maps Correlate with Structural and Molecular Characteristics of Focal Fibrosis**

Mihaela Pop<sup>1,2(✉)</sup>, Samuel Oduneye<sup>1,2</sup>, Li Zhang<sup>1,2</sup>, Susan Newbigging<sup>3</sup>,  
and Graham Wright<sup>1,2</sup>

<sup>1</sup> Sunnybrook Research Institute, Toronto, Canada  
mihaela.pop@utoronto.ca

<sup>2</sup> Medical Biophysics, University of Toronto, Toronto, Canada

<sup>3</sup> Centre for Modelling of Human Disease (CMHD) - Pathology Core,  
Toronto Centre for Phenogenomics, Toronto, Canada

**Abstract.** The purpose of this work was to use noninvasive *in vivo* MRI to characterize the substrate (i.e., known as *gray zone*, GZ) of ventricular arrhythmia, a major cause of sudden death. Our aim was to use a preclinical model of chronic infarction to study the structural and molecular characteristics of infarcted areas. For this, we related parametric T<sub>1</sub> maps with the density of collagen and gap junctions (Cx43 proteins) in patchy fibrosis in n = 6 swine with chronic infarction. Specifically, *in vivo* T<sub>1</sub> relaxation maps were calculated from 2D multi-contrast late enhancement (MCLE) MR images obtained at 1 × 1 × 5 mm resolution. Quantitative analysis and regression analysis demonstrated that the comparison between GZ and scar extent in MCLE to the corresponding areas identified in histology, yielded very good correlations in both cases (i.e., goodness of fit: R<sup>2</sup> = 0.89 for GZ, and 0.92 for dense scar, respectively). Furthermore, the gap junction Cx43 density was significantly reduced (i.e., by > 50%) in the ischemic GZ areas determined from MCLE. These novel results suggest that *in vivo* 2D parametric T<sub>1</sub> maps can be used to evaluate the biophysical properties of healing myocardium post-infarction, and to distinguish between the infarct categories (i.e., scar vs. GZ) with re-modelled structural and electrical characteristics.

**Keywords:** Myocardial infarct · Cardiac MRI · T1 maps · Gray zone · Fibrosis · Gap junctions

## **1 Introduction**

The arrhythmogenic substrate for potentially lethal heart rhythms in patients with prior myocardial infarction is typically located in the peri-infarct, or so-called *gray zone* (GZ), which is found between the normal tissue and dense scar (i.e., mature collagen that replaced dead tissue during healing) [1]. GZ is comprised of a mixture of viable myocytes and collagen fibers, and has altered electrical properties (i.e., this tissue conducts the action potential wave slower than normal tissue) [2]. Currently, in the electrophysiology (EP) lab, the chronic infarct areas are identified using invasive electro-anatomical mapping. However, although the electrical signals help identify some of the

arrhythmogenic foci, the voltage maps are recorded only from the surface and do not provide transmural information [3]. Thus, an important task for the clinicians is to determine the location, extent and transmural extent of infarction, and this is often done non-invasively by employing contrast-based MRI methods [4]. The conventional late gadolinium LGE MR imaging method is based on the elevation of signal intensity (SI) values within infarct regions, measured ~15 min after the contrast agent injection. The enhancement is due to different concentrations and kinetics of the Gd-based molecules in the extracellular space within the infarct (scar/GZ), where they shorten the  $T_1$  relaxation time [5]. As a result, the infarct appears brighter than the healthy myocardium, other surrounding tissues and the blood.

To date, several studies fused LGE and EP maps, showing that critical sites of scar-related arrhythmias are confined to areas of elevated signal intensity (SI) in LGE images [6, 7]. However, they also suggested that discrepancies between GZ detected by LGE and EP maps could be due to: far-field influences from normal tissue, manual delineation of scar, and poor wall-catheter contact during EP mapping. In most of these LGE studies, SI threshold was set at 2–3 SD (standard deviation) higher than the mean SI selected from remote myocardium [8]. However, this algorithm is affected by noise, which is inherent in the MR signal. The noise in the inversion recovery gradient echo (IR-GRE) image plays a large role in determining the measured SI; thus, by changing the location of the remote region, the SD and peak SI can vary significantly due to a repeated sampling of the noise whose distribution has a large variance. This leads to different SI cut-off values for defining the scar and GZ, resulting in a high variability of the GZ size and less reproducible results. An alternative method involves our  $T_1$ -mapping method based on multi-contrast late enhancement MCLE, which employs a simultaneous nulling of MR signal from healthy tissue and blood for better identification of sub-endocardial lesions, has superior SNR compared to LGE and outperforms the SD and FWHM-based segmentation algorithms [9].

To date, there is no quantitative study demonstrating the relation between *in vivo*  $T_1^*$  parametric maps and quantitative histopathology. Thus, the purpose of this paper was to better characterize the heterogeneous fibrosis (i.e., dense scar and GZ) using a pre-clinical swine model of chronic infarction by employing an *in vivo* 2D MCLE imaging method that uses steady-state free precession SSFP readouts, along with quantitative histopathology (i.e., density of collagen in the fibrotic areas, and density of gap junctions Cx43 responsible for electrical connections between myocardial cells). Such investigation might provide a better characterization of structural and molecular characteristics of the collagenous scar and ischemic GZ (i.e., the arrhythmogenic substrate).

## 2 Materials and Methods

A simplified diagram of the proposed framework is shown in Fig. 1. Briefly, we first acquired the *in vivo* MCLE data, followed by data post-processing (i.e., LV segmentation and tissue clustering into: healthy area, scar and GZ). Lastly, using histopathological and Cx43 fluorescence images we analyzed the density of collagen and gap junctions, and then related these measures with the segmented  $T_1^*$  parametric maps.

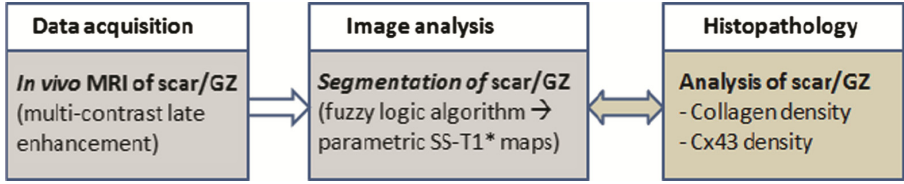


**Fig. 1.** Schematic diagram of the work-flow

## 2.1 Animal Model of Infarction and *in Vivo* MRI Study

All animal experiments included in this pre-clinical framework were approved by our research institute. The myocardial infarction was generated in  $n = 6$  swine using an occlusion-reperfusion method as previously described in other studies [10]. The infarct lesions were allowed to heal for 5–6 weeks.

The MR imaging studies were performed on a dedicated 1.5T research scanner (GE SignaExcite) using a 5-inch surface coil. The MR scans had the following parameters: TE = 1.9 ms, TR = 5.5 ms, NEX = 1, FOV = 26 cm,  $256 \times 256$  acquisition matrix. The spatial resolution was  $1 \times 1 \times 5$  mm. Late enhancement imaging was started 10–15 min after the injection of 0.2 mmol/kg of Gd-DTPA. Several short-axis MCLE images were acquired through the infarct volume, with the inversion pulse placed such that the infarct-enhanced images were acquired with minimal motion during diastole, for which TI (inversion time) ranged from 175 to 250 ms.

The MCLE used SSFP readouts during the inversion recovery IR process, producing 20 images over the cardiac cycle. Notably, the MCLE images at early inversion times have varying contrast where the infarct can be visualized as an area of fast  $T_1^*$  recovery. Moreover, the observed  $T_1^*$  is usually shorter than the intrinsic  $T_1$  relaxation time due to the nature of the b-SSFP measurement (readout), with the magnetization recovering to a steady-state (SS) value. Figures 2a–f show six (out of 20) MCLE images corresponding to one 2D short-axis MR slice in one of the animals studied. Approximately 6–8 images per heart cycle (in diastole) were selected and then used to extract the SI recovery curve for each pixel within the LV (including the blood pool pixels), given that SI obeys the Eq. (1):

$$SI(\text{time}) = SS \cdot [1 - 2\exp(-\text{time}/T_1^*)] \quad (1)$$

Specifically,  $T_1^*$  depends on the longitudinal relaxation  $T_1$ , the transverse relaxation  $T_2$  and the flip angle  $\alpha$  (i.e. the angle to which the net magnetization is tipped relative to the direction of main magnetic field after the application of an RF excitation pulse at Larmor frequency), as per the following equation [11]:

$$T_1^* = \left( \frac{1}{T_1} \cos^2 \frac{\alpha}{2} + \frac{1}{T_2} \sin^2 \frac{\alpha}{2} \right)^{-1} \quad (2)$$

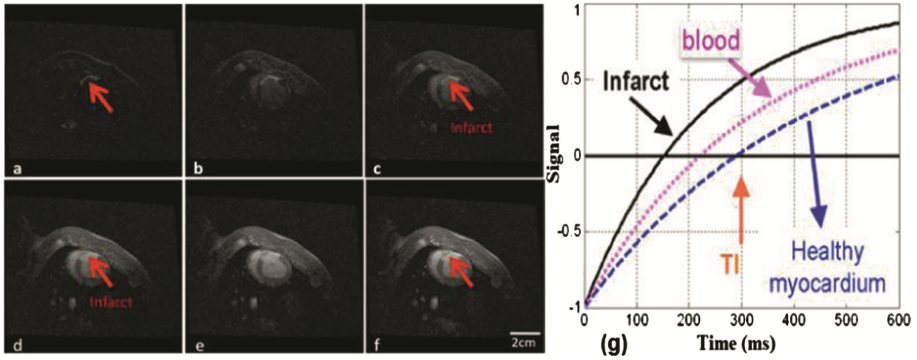


**Fig. 2.** Example of MCLE imaging in a pig with an LAD-infarct: (a–f) six consecutive short-axis MCLE images (the infarct is visualized as a hyper-enhanced region as indicated by arrow); (g) SI recovery plotted from three pixels (different tissue types).

The plot in Fig. 2g shows an example of the SI recovery based on Eq. (1), obtained in three different pixels from the infarct, blood and healthy myocardium, respectively (using a three-parameter fitting and a smooth function in Matlab).

## 2.2 Data Processing: Tissue Segmentation and Parametric $T_1^*$ -SS Maps

For the 2D MCLE images, a corresponding spatial map of various tissue types in LV was generated using an in-house developed fuzzy clustering analysis (in Matlab). This algorithm determined the probability of each pixel belonging to each of the 3 clusters, based on a distance metric derived from the scatter plot of  $T_1^*$  versus steady-state (SS). A scatter plot of  $T_1^*$  versus SS value for each pixel was then used as input to a fuzzy C-means algorithm, and automatically classified each pixel as: either infarct, or healthy myocardium, or blood.

The FCM algorithm was based on the Gustav-Kessel (GK) clustering method, a robust tool used in system identification and in particular in some classification problems where it is desired to implement a local adjustment of the distance metric to the geometrical shape of the cluster(s). The main characteristic of the GK scheme is the estimation of the cluster covariance matrix and the distance-induce matrix. This was done here by optimizing an objective FCM-type of function using the *Fuzzy-logic Matlab toolbox*. For tissue segmentation we determined the probability of each pixel belonging to a cluster using the distance metric derived from the input SS- $T_1^*$  scatter plot. The pixels with probabilities  $> 75\%$  of belonging to infarct or healthy tissue were classified as *dense scar* and *healthy myocardium*, respectively. Furthermore, the pixels classified as *GZ* (the mixture of dead and viable myocytes) had a significant probability for belonging to both the healthy and infarct clusters (less than a 75% probability of belonging to one of those clusters and greater than 25% probability for belonging to the other cluster).

### 2.3 Quantitative Histopathology Analysis

For histology, a total of  $N = 10$  tissue slices (5-mm) were cut from each heart (1–2 slices/heart), matching short-axis MCLE images. The samples were fixed in 10% formalin and embedded in paraffin for a few days, avoiding excessive shrinking.

First, thin slices (4–5  $\mu\text{m}$ ) underwent whole-mount staining on large glass slides, using collagen-sensitive stain Picrosirius Red, PR. The slides were scanned with a TISSUEScope<sup>TM</sup> 4000 confocal system (Huron Technologies International Inc.), saved as multi-resolution digital images and analyzed with the Aperio Image Scope software (Vista, CA). The GZ and scar areas were manually delineated by pathology expert (Fig. 3) based on score for fibrosis severity as in [12]. We defined three grades of fibrosis for our tissue types: F0 ( $< 20\%$  fibrosis, *no or mild*) for healthy/normal myocardium (in remote areas); F1 ( $20\text{--}70\%$  fibrosis, *moderate*) for GZ; and, F2 ( $\geq 70\%$  fibrosis, *severe*) for scar.

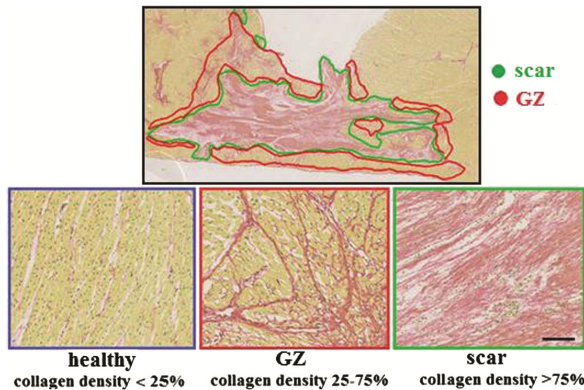
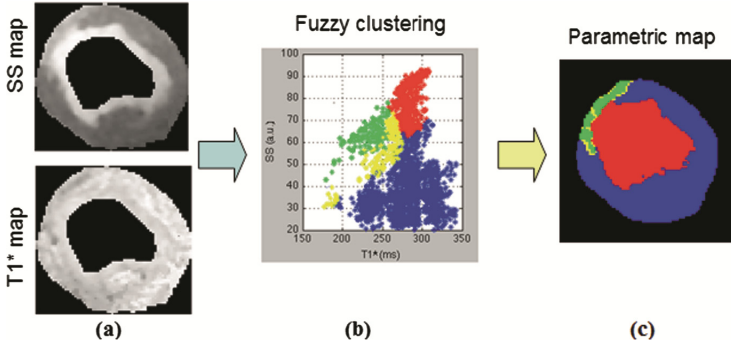


**Fig. 3.** Histopathology in an infarcted pig heart. Example of manual tissue segmentation (healthy zone, GZ and dense scar) based on grading fibrosis using collagen-sensitive P.R. stain (note: collagen stains red and the healthy myocytes stain yellow). (Color figure online)

Note that for the correlation between the scar and GZ areas (relative to LV area) and the corresponding areas obtained from the SS-T1\* maps, we manually registered the histological and MR images via anatomical markers (e.g. RV/LV insertion points, papillary muscle, etc.), which were clearly visible in both type of images. Second, select samples were also prepared for fluorescence microscopic imaging of Cx43 as in [13], and scanned with a Hamamatsu scanner. The density of Cx43 was quantified using the Visiopharm software ([www.visiopharm.com](http://www.visiopharm.com)). ROIs were selected from zones defined as: healthy tissue, GZ and scar in the SS-T1\* maps and collagen-based stains. We investigated the changes in cell-to-cell coupling (in the longitudinal direction of myocytes) and side-to-side coupling (in the transverse direction of myocytes). The software calculates the area stained for Cx43 in microscopy fluorescence images in a ROI (where myocytes stain in green and the gap junctions stain in red) relative to the area of that selected ROI. Here we used ROIs of  $2 \times 2$  mm.

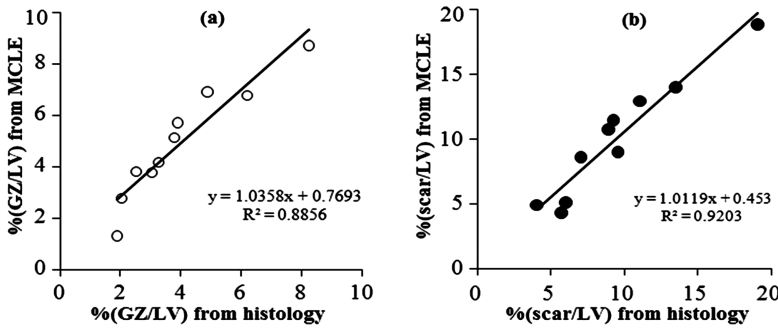
### 3 Results

Figure 4 shows a representative result from the analysis of MCLE images in one pig. SS image and  $T_1^*$  map are shown in Fig. 4a. Figure 4b shows a scatter plot of  $T_1^*$  vs. SS values for all pixels within the LV. The resulted 2D spatial map of various tissue types classified using the fuzzy clustering algorithm is shown in Fig. 4c: dense scar (green), BZ (yellow), healthy tissue (blue), and blood (red).



**Fig. 4.** Representative results obtained in a swine heart with an LAD-infarct: (a) SS image (*up*) and  $T_1^*$  map (*bottom*); (b) fuzzy clustering scatter plot of  $T_1^*$  vs. SS values for all pixels within the LV; and, (c) corresponding 2D parametric map of various tissue categories classified by the fuzzy clustering algorithm.

Figure 5 shows the quantitative comparison between % GZ area (a) and dense scar (b) relative to LV area, as determined pixel-by-pixel from *in vivo* MCLE and histology. The regression analysis and linear fit yielded very good correlation in both cases (goodness of fit:  $R^2 = 0.89$  for GZ, and 0.92 for scar, respectively).



**Fig. 5.** Correlation between GZ (a) and scar areas (b) relative to LV area determined from 2D parametric SS- $T_1^*$  maps and collagen-sensitive stains.

Figure 6 shows an example of fluorescence image at 40x magnification (myocytes stain green and Cx43 red). All samples contained healthy myocardial tissue, GZ and

scar (see Fig. 6a). The connexin Cx43 (red dots) were clustered at the intercalated disks of myocytes. All ROIs analyzed quantitatively (see magnified images in Fig. 6b and 6c) were selected from MCLE-derived healthy, GZ and scar zones. Qualitatively, there was an apparent reduction in Cx43 density in the GZ compared to healthy tissue in both longitudinal (*up*) and transverse (*bottom*) directions. The connexin Cx43 was completely inhibited in the collagenous scar (images not included). Notable also was a clear increased extra-cellular space and cellular disconnection in GZ due to collagenous fibrils separating viable myocytes.

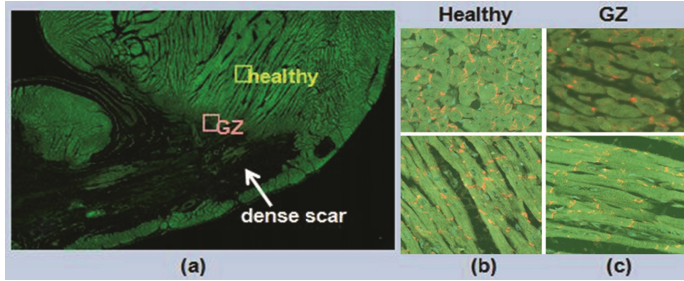


**Fig. 6.** Qualitative fluorescence microscopy images of Cx43 (see text for details).

Furthermore, as seen in Fig. 7, the quantitative analysis demonstrated a significant reduction ( $> 50\%$ ) in Cx43 density in the ventricular peri-infarct (GZ) in both longitudinal and transverse directions of myocytes, compared to the Cx43 density in the healthy tissue. This reduction may contribute to the electrical uncoupling of myocytes (resulting in slower conduction of impulse) and formation of arrhythmia substrate.

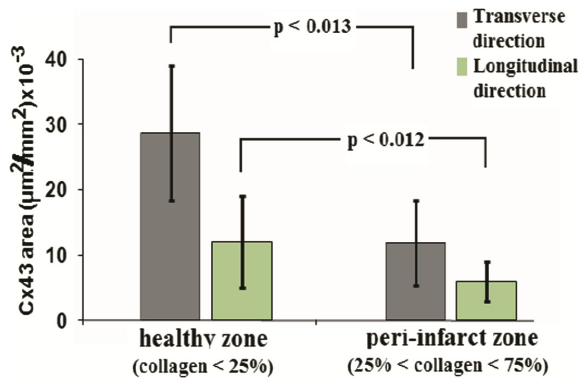


**Fig. 7.** Quantitative analysis for gap junctions: comparison of Cx43 density in the GZ and healthy tissue, for both longitudinal and transverse directions of myocytes (significant differences denoted by  $p$  values  $< 0.05$ ).



## 4 Discussion

Accurate characterization of chronic infarct remodelling is an important task in order to identify substrate of potentially lethal ventricular arrhythmia (VT/VF). This clearly motivates the development of pre-clinical experimental frameworks and advanced technologies based on non-invasive imaging methods as MCLE, which can offer rich transmural and structural information to supplement the invasive, sparse and surfacic electrophysiological measurements. Using MCLE, one can generate accurate SS- $T_1^*$  parametric maps that advantageously may be used to detect infarcted tissue without the need to estimate the TI for nulling myocardium as in LGE methods.

Our study is the first to evaluate quantitatively the relation between MR tissue properties based on *in vivo*  $T_1^*$  relaxation maps and the density of collagen in chronic fibrosis. Overall, the comparison between MCLE-derived GZ and scar areas vs. histologically-derived GZ and scar areas, demonstrated that 2D SS- $T_1^*$  parametric maps provided an accurate classification of infarct heterogeneities and identified subtle sub-endocardial lesions at the tissue-blood interface. The  $T_1$ -like maps reflected the structural changes in focal fibrosis, showing an increase in extracellular space and collagen deposition in the healing infarct, as well as the presence of patchy fibrosis (a hallmark of the substrate for lethal VT/VF).

We acknowledge that a limitation of this study is the relatively small sample size (i.e.,  $n = 6$  animals with chronic myocardial infarction), that is because such *in vivo* preclinical experiments are expensive and difficult to perform, while whole-mount histology is laborious and expensive. However, the 10 histological tissue samples provided sufficient data points for an accurate statistical analysis and to obtain very good correlation between the pixel-by-pixel MCLE-derived GZ/scar areas and collagen-defined GZ/scar areas. The slightly poorer goodness of fit for GZ compared to scar can be explained by the partial volume effect in the peri-infarct area, and was due to the mixture of viable and non-viable myocytes (which contributed to an average value of  $T_1^*$  within the 5 mm slice thickness).

The structural changes in fibrotic areas were accompanied by alterations at molecular level as indicated by inhibition of the Cx43 protein, a major ventricular gap junction that facilitates the flow of ionic current between the cells [3]. Our results showed that Cx43 density was significantly reduced in the ischemic GZ by  $> 50\%$  in both directions of the myocytes (longitudinal and transverse), which could trigger delayed propagation of activation wave [14]. The closure of connexin Cx43 in the ischemic GZ is important because it reduces the conduction velocity in the arrhythmogenic substrate and facilitates the triggering of VT/VF [15].

To conclude, *in vivo* 2D SS- $T_1^*$  maps enabled accurate MR probing of remodelled myocardium. Such maps can be used to evaluate the changes in structural and molecular characteristics with focal fibrosis, and to distinguish between myocardial tissue categories (i.e., dense scar vs. GZ). Future work will focus on improving the MCLE segmentation algorithm and compare it to other intensity-based segmentation methods. Also, we hope to improve the comparison between tissue categories as defined by MRI and histology, by performing a non-rigid registration between the MCLE images and the



whole-mount stained slides. Lastly, as per preliminary results presented in [16], we will continue to improve the *in vivo* spatial resolution of MCLE images and further develop accurate 3D MCLE-based heart models to predict the inducibility of scar-related VT through *in silico* simulations.

**Acknowledgement.** The authors would like to thank preclinical veterinary technicians at Sunnybrook for help with the infarct creation and MR studies. This work was financially supported by a CIHR grant (MOP #93531).

## References

1. Ursell, P.C., Gardner, P.I., Albala, A., Fenoglio, J., Wit, A.L.: Structural and electrophysiological changes in the epicardial border zone of canine myocardial infarcts during infarct healing. *Circ. Res.* **56**, 436–451 (1985)
2. Bolick, D., Hackel, D., Reimer, K., Ideker, R.: Quantitative analysis of myocardial infarct structure in patients with ventricular tachycardia. *Circulation* **74**(6), 1266 (1986)
3. Janse, M.J., Wit, A.L.: Electrophysiological mechanisms of ventricular arrhythmias resulting from myocardial ischemia and infarction. *Physiol. Rev.* **69**(4), 1049–1169 (1989)
4. Bello, D., Fieno, D.S., Kim, R.J., et al.: Infarct morphology identifies patients with substrate for sustained ventricular tachycardia. *J. Am. Coll. Cardiol.* **45**(7), 1104–1110 (2005)
5. Kim, R.J., Fieno, D.S., Parrish, T.B., Harris, K., Chen, E.L., Simonetti, O., Bundy, J., Finn, J.P., Klocke, F.J., Judd, R.M.: Relationship of MRI delayed contrast enhancement to irreversible injury, infarct age, and contractile function. *Circulation* **100**, 1992–2002 (1999)
6. Codreanu, A., Odille, F., Aliot, E., et al.: Electro-anatomic characterization of post-infarct scars comparison with 3D myocardial scar reconstruction based on MR imaging. *J. Am. Coll. Cardiol.* **52**, 839–842 (2008)
7. Wijnmaalen, A., van der Geest, R., van Huls van Taxis, C., Siebelink, H., Kroft, L., Bax, J., Reiber, J., Schalij, M., Zeppenfeld, K.: Head-to-head comparison of contrast-enhanced magnetic resonance imaging and electroanatomical voltage mapping to assess post-infarct scar characteristics in patients with ventricular tachycardias: Real-time image integration and reversed registration. *Eur. Heart J.* **32**(1), 104–114 (2011)
8. Roes, S.D., Borleffs, C.J., van der Geest, R.J., et al.: Infarct tissue heterogeneity assessed with contrast-enhanced MRI predicts spontaneous ventricular arrhythmia in patients with ischemic cardiomyopathy and implantable cardioverter-defibrillator. *Circ. Cardiovasc. Imaging* **2**, 183–190 (2009)
9. Detsky, J.S., Paul, G., Dick, A.J., Wright, G.A.: Reproducible classification of infarct heterogeneity using fuzzy clustering on multicontrast delayed enhancement magnetic resonance images. *IEEE Trans. Med. Imaging* **28**(10), 1606–1614 (2009)
10. Pop, M., Ramanan, V., Yang, F., Zhang, L., Newbigging, S., Ghugre, N., Wright, G.A.: High resolution 3D T1\* mapping and quantitative image analysis of the gray zone in chronic fibrosis. *IEEE Trans. Biomed. Eng.* **61**(12), 2930–2938 (2014)
11. Salerno, M., Janardhanan, R., Jiji, R.S., Brooks, J., Adenaw, N., Mehta, B., Yang, Y., Antkowiak, P., Kramer, C.M., Epstein, F.H.: Comparison of methods for determining the partition coefficient of gadolinium in the myocardium using T1 mapping. *J. Magn. Reson. Imaging* **38**(1), 217–224 (2013)
12. Pop, M., Ghugre, N.R., Ramanan, V., Morikawa, L., Stanis, G., Dick, A.J., Wright, G.A.: Quantification of fibrosis in infarcted swine hearts by ex vivo late gadolinium-enhancement and diffusion-weighted MRI methods. *Phys. Med. Biol.* **58**(15), 5009 (2013)

13. Jansen, J., van Veen, T., de Jong, S., van der Nagel, R., van Stuijvenberg, L., Driessen, H., Labzowsky, R., Oefner, C.M., Bosch, A., Nguyen, T.Q., Goldschmeding, R., Vos, M.A., de Bakker, J.M.T., van Rijen, H.: Reduced Cx43 expression triggers increased fibrosis due to enhanced fibroblast activity. *Circ. Arrhythmias Electrophysiol.* **5**(2), 380–391 (2012)
14. Kawara, T., Derksen, R., de Groot, J.R., Coronel, R., Tasseron, S., Janse, M.J., de Bakker, M.J.: Activation delay after premature stimulation in chronically diseased myocardium relates to architecture of interstitial fibrosis. *Circulation* **104**, 3069–3075 (2001)
15. Stevenson, W.G.: Ventricular scars and VT tachycardia. *Trans. Am. Clin. Assoc.* **120**, 403–412 (2009)
16. Zhang, L., Athavale, P., Pop, M., Wright, G.A.: Multi-contrast reconstruction using compressed sensing with low rank and spatially-varying edge-preserving constraints for high-resolution MR characterization of myocardial infarction. *Magn. Reson. Med.*, September 2016, in press. (doi:[10.1002/mrm.26402](https://doi.org/10.1002/mrm.26402))

Functional Imaging and Modelling of the Heart  
9th International Conference, FIMH 2017, Toronto, ON,  
Canada, June 11-13, 2017, Proceedings  
Pop, M.; Wright, G. (Eds.)  
2017, XVI, 517 p. 233 illus., Softcover  
ISBN: 978-3-319-59447-7